Article

Comparing the Dry Season *In-Situ* Leaf Area Index (LAI) Derived from High-Resolution RapidEye Imagery with MODIS LAI in a Namibian Savanna

Manuel J. Mayr [1],* and Cyrus Samimi [1,2]

[1] Department of Geography, University of Bayreuth, Universitätsstr. 30, 95447 Bayreuth, Germany; E-Mail: cyrus.samimi@uni-bayreuth.de

[2] Bayreuth Center of Ecology and Environmental Research (BAYCEER), University of Bayreuth, Dr. Hans-Frisch-Str. 1-3, 95448 Bayreuth, Germany

* Author to whom correspondence should be addressed; E-Mail: manuel.mayr@uni-bayreuth.de; Tel.: +49-921-554-656; Fax: +49-921-552-314.

Abstract: The Leaf Area Index (LAI) is one of the most frequently applied measures to characterize vegetation and its dynamics and functions with remote sensing. Satellite missions, such as NASA's Moderate Resolution Imaging Spectroradiometer (MODIS) operationally produce global datasets of LAI. Due to their role as an input to large-scale modeling activities, evaluation and verification of such datasets are of high importance. In this context, savannas appear to be underrepresented with regards to their heterogeneous appearance (e.g., tree/grass-ratio, seasonality). Here, we aim to examine the LAI in a heterogeneous savanna ecosystem located in Namibia's Owamboland during the dry season. Ground measurements of LAI are used to derive a high-resolution LAI model with RapidEye satellite data. This model is related to the corresponding MODIS LAI/FPAR (Fraction of Absorbed Photosynthetically Active Radiation) scene (MOD15A2) in order to evaluate its performance at the intended annual minimum during the dry season. Based on a field survey we first assessed vegetation patterns from species composition and elevation for 109 sites. Secondly, we measured *in situ* LAI to quantitatively estimate the available vegetation (mean = 0.28). Green LAI samples were then empirically modeled (LAI$_{model}$) with high resolution RapidEye imagery derived Difference Vegetation Index (DVI) using a linear regression ($R^2 = 0.71$). As indicated by several measures of model performance, the comparison with MOD15A2 revealed moderate consistency mostly due to overestimation by the aggregated LAI$_{model}$.

Model constraints aside, this study may point to important issues for MOD15A2 in savannas concerning the underlying MODIS Land Cover product (MCD12Q1) and a potential adjustment by means of the MODIS Burned Area product (MCD45A1).

1. Introduction

Savannas are characterized as ecosystems where the co-existence of woody and grass species is moderated by resources and disturbances. One hypothesis in this context is that different phenological cycles of woody and herbaceous species are one reason for their co-existence [1,2]. Deep-root water uptake allows woody species to initiate early leaf expansion and to prolong the leaves into the dry season. Contrarily, grass growth is stimulated by the first precipitation events yet they wither as soon as near-surface water vanishes. Thus, the general term "growing season" appears imprecise for such regions [3].

The Leaf Area Index (LAI) is a quantitative measure of the green vegetation available per surface area. Hence, it is a proxy for the above-mentioned phenological cycles. Several definitions exist (*cf.* [4]), they typically vary according to the field of application of LAI (e.g., vegetation growth and phenology, potential physiological activity, light attenuation under plant canopies). Of these, a widely acknowledged definition of LAI is the one-sided, or hemi-surface, leaf area per unit of the horizontal land below. Besides being a proxy for plant growth the LAI is an important biophysical parameter for the interaction between plants and the atmosphere because processes like photosynthesis and evapotranspiration are linked to LAI [5,6]. Thus, the LAI is often used to model and monitor evapotranspiration, Net Primary Production (NPP) and Net Ecosystem Exchange (NEE) at different scales (e.g., [7–10]).

Such applications require LAI in a sufficient medium to high resolution [8,9], which could be derived with ground-based methods and through remote sensing, only the latter allowing LAI estimates for larger regions in a cost effective way. For monitoring purposes, a high temporal resolution as provided by MODIS is critical. Hence, often a combination of different spatial and temporal resolutions is needed, which requires validation and up-scaling [11].

In this context, ground-based methods for assessing LAI are essential. They include (semi-)direct, such as harvesting of leaves or allometric relationships, and indirect approaches [12]. The predominant benefits of indirect methods arise from their non-destructive nature and an increased spatial sampling rate, whereas direct methods are considered the most reliable measurements [13]. With indirect methods, the spatial heterogeneity of canopy elements is inferred using photosensitive instruments, which either record the transmitted radiation at multiple points (multi-sensor array) or from a single sensor with angular capacity [13]. Sensors with angular capacity most frequently apply the concept of gap fraction, *i.e.*, the fraction of sky visible from below a canopy in any specific direction, in order to determine canopy gaps [14]. The actual derivation of LAI is subsequently achieved by inversion and the application of a light extinction model [13]. Such models relate the recorded transmission of radiation through a canopy to idealized, randomly arranged canopy architecture [14,15]. In real canopies, however, leaf inclination angles are species-specific and often reflect phenology, whereas clumping of foliage is

initially caused by plant morphology. Van Gardingen *et al.* [16] report that clumping alone may reduce indirect estimates of LAI by up to 50%. Consequently, Chen & Black [17] introduced the term "effective LAI" (LAI$_{eff}$) for optically derived LAI. Furthermore, most optical devices fail to discriminate green tissue from other canopy elements (Stem or Woody Area Index (SAI, WAI, respectively)), which actually leads to a plant area index (PAI) [12,18].

LAI can also be estimated using remote sensing techniques with the advantage of increased spatial sampling. Here, LAI is mapped based on the relationship between *in situ* samples and spectral information sensitive to vegetation. However, such empirical-statistical models lack transferability to other regions due to varying atmospheric and surface conditions as well as the sensor-view sun conditions [19]. Nevertheless, their application on a regional scale is justified through their simplicity and subsequent short computational times [20].

Earth-observation systems, such as NASA's Moderate Resolution Imaging Spectroradiometer (MODIS) mission, operationally produce global LAI datasets (MOD15A2). These datasets are generated using the physical approach, *i.e.*, Radiative Transfer Models (RTM) that link surface reflectance (output) with the structural parameters of a canopy (input) through a set of approximations for canopy architecture, leaf properties, and the sensor-view sun conditions [6,20]. The actual derivation of a biophysical variable is achieved through RTM model inversion. Several uncertainties are associated with the physical approach, and summarized by Garrigues *et al.* [6]. The accuracy of datasets such as MOD15A2 is critical for the applications that use these. Hence, many efforts have been put into the evaluation and validation of MOD15A2 for different biomes (e.g., [21–26]). A direct validation of MODIS with ground measurements is not possible because of scale differences. Hence, validation studies often use high to medium resolution datasets to scale up *in situ* LAI. The derived datasets are then again scaled up to allow for a comparison with MOD15A2 [23,26].

Independent of the method applied, the determination of LAI in savannas is a complex task, yet relatively few studies have focused on the inaccuracies that arise from high heterogeneity and small-scale patchiness in such ecosystems [27]. Furthermore, phenological aspects are often neglected in studies assessing LAI [18]. Remote sensing applications traditionally focus on green vegetation for practical reasons. Phenology and senescent vegetation as structural and functional components of ecosystem dynamics seem to be gaining more attention recently [28]. Furthermore, dry-season grass and litter availability are especially important in savanna ecosystems, as they serve as the fine fuels that promote seasonally occurring fires [29].

Thus, the objectives of this paper are to:

(1). Assess ground-based dry-season LAI in a Namibian savanna ecosystem;
(2). upscale LAI field measurements to high-resolution RapidEye imagery;
(3). and compare an *in situ*-calibrated model of LAI with the MODIS LAI product (MOD15A2) in order to evaluate its performance.

2. Study Area

The region of interest covers an area of about 2915 km^2 in the Ovamboland, situated in Northern-Central Namibia (*cf.* Figure 1). According to Mendelsohn *et al.* [30], the region's climate is classified as semi-arid with precipitation being restricted to the austral summer months due to a seasonal

shift of the Congo Air Boundary and the establishment of a stable high-pressure cell over Southern Africa during the austral winter. Mean annual precipitation (MAP) in the region varies between 400 and 500 mm [30]. Aside from distinct inter-annual variability of local precipitation, the region's hydrological regime is predominantly controlled by the rivers of the Cuvelai-Iishana system, which originate in the Encoco Highlands of Angola (MAP ~800 mm) [30]. As a consequence of the topography, the seasonal waters of the Cuvelai spread and meander southwards from the Angolan-Namibian border in channels (known as Iishana) forming a delta-like network that repeatedly experiences devastating floods towards the end of the rainy season [31]. The interplay of alternating drought and flood, together with the highest solar irradiance rates throughout Namibia, explain why salinity is a major issue in the region [32]. Aside from the environmental conditions, human activities, and especially high livestock densities, have a considerable role in the formation of patterns in, as well as the composition of the edaphic grasslands and shrub lands around the Iishana.
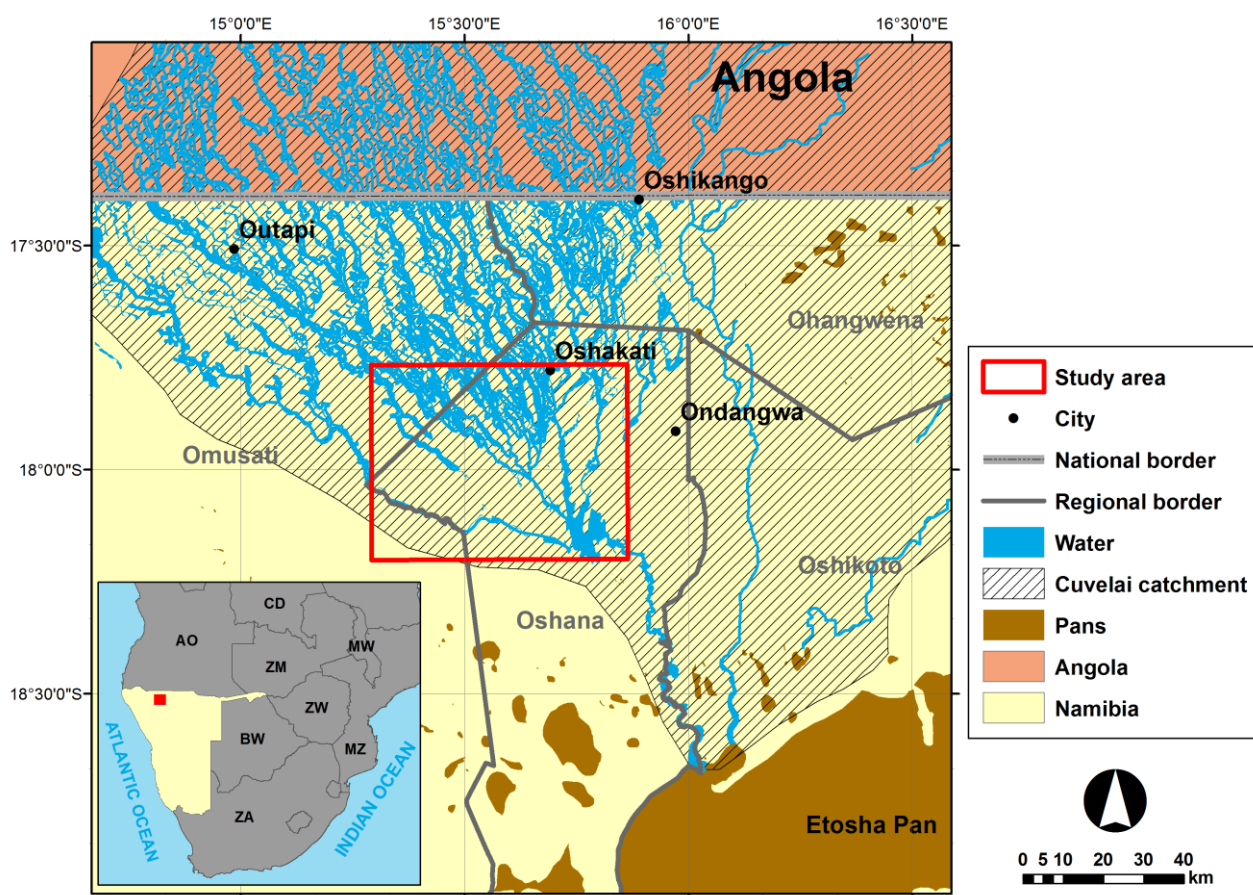
Figure 1. Map of Northern-Central Namibia illustrating the study area and the Cuvelai catchment.

3. Materials and Methods

3.1. Remote Sensing Data

3.1.1. RapidEye

The RapidEye mission consists of five satellites, which provide a 5 m-spatial resolution and cover the three visible bands (blue: 440–510 nm, green: 520–590 nm, red: 630–685 nm), a red-edge (RE) band

(690–730 nm), and a near-infrared (NIR) band (760–850 nm) [33]. A set of "RapidEye Ortho-Level 3A" scenes, acquired on 10 November 2010, was used in this study. These data are delivered with radiometric, sensor, and geometric corrections already applied and assigned to UTM projection (Zone 33S) with WGS 84 datum. No *post hoc* atmospheric correction was performed, because it is not improving results for single date images [34]. Digital numbers (DN) were converted to values of top-of-atmosphere radiance following the RapidEye Product Specifications [33] and, subsequently, to at-ground reflectances by applying the equations given in Mather & Koch [35].

3.1.2. MODIS

Since 2007, the most recent version, "Collection 5" of the MODIS LAI/FPAR product (MOD15A2) has been available. Compared to the preceding "Collection 4", the land cover map (an aggregated scheme of the MODIS Land Cover product (MCD12Q1)) used for parameterization of the look-up-tables (LUT) has been modified. Thus, the biome-specific estimation of LAI is now expanded from six to eight [36]. Furthermore, the LUTs were recalculated using a new stochastic RTM [37]. This refinement of the main algorithm is expected to enhance "high quality" LAI retrievals. "Collection 5" is also the first to provide quality indication measures such as the standard deviation of LAI per pixel, *i.e.*, the accuracy of solutions as retrieved by the main algorithm [38], and a quality control (QC) layer providing information about the emergence of a pixel value (e.g., main or empirical back-up retrieval algorithm, cloud contamination, *etc.*).

A MOD15A2-scene covering an 8-day period from 9 to 16 November 2010, was the best temporal match to the RapidEye image. This scene was obtained from the "USGS MODIS Reprojection Tool Web Interface" (accessible via: mrtweb.cr.usgs.gov) in order to ensure the data were available in the same coordinate system as the RapidEye images. Further processing steps included clipping to the extent of the study area and applying the scale factor (DN × 0.1) for the derivation of LAI values. The information contained by the supplied MOD15A2-QC layer revealed mainly high quality retrievals.

3.2. Field Data

3.2.1. Site Selection

During a field survey at the end of the dry season in October and November 2010 the transitional period of the vegetation prior to the first rains was assessed. In order to determine typical vegetation attributes and phenological status Functional Landscape Units (FLU) of vegetation and landscape parameters were sampled. Functional entities are generally dependent on scale and thus subject to complication by the fuzzy nature of ecological boundaries and gradients [39]. As the field data was also intended to serve as the ground-truth for the remote sensing data, scale had to be considered in relation to the spatial resolution of the RapidEye images, especially with regards to areas of relative homogeneity. Such sampling is referred to as "nested", as the scale of observation determines the perception of an entity [40]. Representative plots of at least 30 × 30 m (6 × 6 pixels) within a FLU and a minimum buffer of 10 m to the adjacent FLU were chosen and geo-located using a GPS. Based on experience in the field, these plots (termed Elementary Sampling Units (ESU)), were preferentially selected via a stratified approach.

3.2.2. Recorded Parameters

In total, data from 109 vegetation covered ESUs were collected. These were mainly located around two sites: (i) IIpopo, and (ii) Omulunga, situated in the central regions of the study area. The vegetation parameters surveyed included: (i) estimated plant cover (in %), (ii) the corresponding relative contribution of the main species for each stratum (if available), (iii) terrain position, and finally (iv) LAI.

3.2.3. Leaf Area Index

Indirect measurements of LAI (hereinafter termed: LAI_{2200}) were conducted for each of the vegetated ESUs using a Li-Cor LAI-2200 Plant Canopy Analyzer device. The sensors record the canopy transmittances of diffuse radiation from above and below canopy records at five concentric zenith angle ranges (centered at 7°, 22°, 38°, 52°, and 68°) in order to derive canopy interception by inversion [41]. For the internal computation of LAI_{2200}, Li-Cor's "horizontal canopy model" (also known as "Poisson model") was used. Here, the radiative transfer through a canopy is described by an extension of the Beer-Lambert law [12]. For a hypothesized canopy with an infinite (and hence infinitely thin) number of statistically independent, horizontal layers the probability of incident light to experience a particular number of contacts with these canopy layers is expressed by a Poisson distribution [42]. Following Weiss *et al.* [5], the probability of no contact (P), or the gap fraction (F), for incident irradiance at any zenith (θ) and azimuth angle (ϑ) is:

$$P(\theta,\vartheta) = F(\theta,\vartheta) = exp\left[\frac{-G(\theta,\vartheta)LAI}{\cos\theta}\right] = exp[-k(\theta,\vartheta)LAI] \tag{1}$$

where $G(\theta,\vartheta)$ is the so-called G-function, which denotes the mean projected area of a unit leaf area in the direction (θ,ϑ). The term $\cos\theta$ accounts for an increased cross-section of canopy to be passed at larger zenith angles [43]. Together the two parameters $G(\theta,\vartheta)$ and $\cos\theta$ form the canopy extinction coefficient ($k(\theta,\vartheta)$).

LAI_{2200} is calculated using the mean contact number ($\overline{K_i}$) and the weighing factors (W_i) for each of the five concentric zenith angles as follows [41]:

$$LAI_{2200} = \int_0^{\pi/2} -\frac{\overline{\ln P(\theta)}}{S(\theta)}\Delta\theta \sin\theta = 2\sum_{i=1}^{5} \overline{K_i} W_i \tag{2}$$

where $S(\theta)$ denotes the path length at the incident angle θ.

Although the "horizontal canopy model" assumes that foliage elements are randomly distributed, the device computes an approximate parameter of the spatial distribution of foliage from its view angles known as the Apparent Clumping Factor (ACF), which, thus, accounts for foliage clumping.

All samples were conducted according to the "Li-Cor LAI-2200 Plant Canopy Analyzer Instruction Manual" [41]. As overcast sky conditions are not existent during the dry season, the sampling predominantly took place at low solar elevation angles as recommended by Kobayashi *et al.* [44]. Additionally, the sensor was always shaded from direct illumination by the operator. A 45° view cap was used to reduce the underestimating influence of canopy gaps [45]. Each LAI_{2200} measurement consisted of at least one reference measurement (above-canopy) and several below-canopy measurements, taken just above the ground. In the sampling scheme, measurements were made at 5 m

intervals along two perpendicularly intersecting transects (*cf.* Figure 2), following a modified systematic approach given in Garrigues *et al.* [46].

The device-internal calculation of LAI$_{2200}$ solely applied the standard settings with the exception of transmittances >1.0. In this case, transmittance values were "clipped" to 1.0 (above-canopy irradiance = below-canopy irradiance), as, especially when using narrow view caps, the possibility of having no vegetation within the sensor's view is present [41].
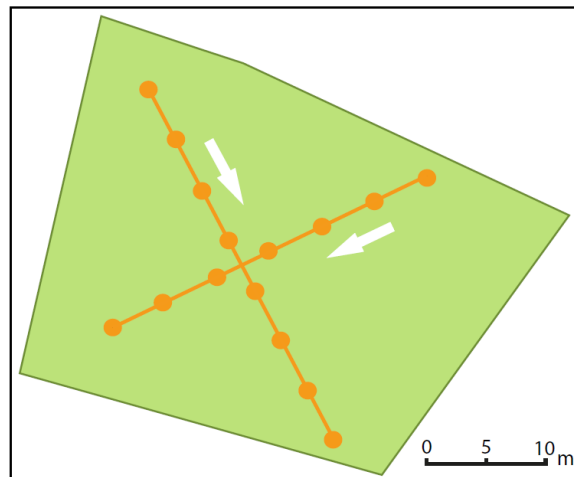
Figure 2. Schematic illustration of spatial sampling for ESU I66: measurements were made at 5 m intervals along two perpendicularly intersecting transects. Points (orange) indicate the 15 measurements below the canopy in ESU I66 (green). Directions of the sampling process are indicated by the white arrows.

3.3. Empirical-Statistical Modeling of LAI

In order to map LAI on a fine scale, it is necessary to establish a statistical relationship between *in situ* measured LAI (LAI$_{2200}$) and the reflectances contained in the RapidEye pixels. Thus, variation in spectral information is assumed to result from variation in LAI only [25]. In reality, this assumption is hampered by a number of uncertainties (e.g., optical and structural species-specific leaf properties, background illumination, topography, and interference of radiation with the atmosphere or sensor viewing geometry) [43]. Numerous Spectral Vegetation Indices (SVI) have been proposed (*cf.* [47] for an overview) in order to minimize external noise and to accentuate the spectral signal of (green) vegetation from non-vegetated surfaces [48].

In a first step, SVIs including RapidEye's RE band and several established SVIs were computed from the band reflectances (Table 1). For each ESU, the mean of the respective SVI was compiled from all pixels where the centroid was contained within the respective ESU. Due to RapidEye's band configuration, only classes of green vegetation ("*open woodland*" and "*Colophospermum mopane shrub land*"; *cf.* Figure 3) could be used in this process. Other ESUs were excluded due to mainly senescent vegetation, or spectral interference from surface heterogeneity (e.g., "*wetlands*"). In order to determine the most accurate relationship between the two parameters, a correlation analysis was performed for the paired observations of LAI$_{2200}$ and respective SVIs. The agreement of the variables was identified using the Coefficient of Determination (R^2). Although the relationship between LAI and SVIs has often been

reported to appear non-linear, as a saturation of the SVI is likely to occur with more dense canopies [15,49], only linear models were tested. This can be justified because sparse vegetation is dominant, and therefore only a small range of LAI_{2200} is represented by the ESUs.

Table 1. Spectral Vegetation Indices (SVI) used in this study. The last four SVIs include the red-edge band of RapidEye.

Spectral Vegetation Index	Equation	Reference
Simple Ratio (SR)	NIR/R	[50]
Difference Vegetation Index (DVI)	$NIR - R$	[51]
Normalized Difference Vegetation Index (NDVI)	$(NIR - R)/(NIR + R)$	[52]
Transformed Vegetation Index (TVI)	$\sqrt{((NIR - R)/(NIR + R) + 0.5)}$	[53]
Soil-adjusted Vegetation Index (SAVI)	$(NIR - R)/(NIR + R + SL)\,(1 + SL)$	[49]
Enhanced Vegetation Index (EVI)	$2\,(NIR - R)/(L + (C_1\,NIR) + (C_2\,R))$	[49]
Simple Ratio (SR $_{NIR/RE}$)	NIR/RE	[54]
Simple Ratio (SR $_{RE/R}$)	RE/R	[54]
Normalized Difference Vegetation Index (NDVI $_{NIR/RE}$)	$(NIR - RE)/(NIR + RE)$	[54]
Normalized Difference Vegetation Index (NDVI $_{RE/R}$)	$(RE - R)/(RE + R)$	-
NOTE: $SL = 0.1$, $L = 1.0$, $C_1 = 6.0$, and $C_2 = 7.5$	-	-

Figure 3. Exemplary sites of green vegetation in the study area: (**left**) *Colophospermum mopane* shrub lands. (**right**) Open woodlands, mainly containing Makalani palms (*Hyphaene petersiana*).

As the estimation of LAI from remote sensing gives "real" LAI values, an absolute value of 0.35 was subtracted *post hoc* from the empirically calibrated LAI_{model}. This aimed to account for the contribution of WAI to the LAI_{2200} samples and was adopted from Privette *et al.* [21], who corrected *in situ* estimates of LAI in a validation study of MOD15A2 in the Kalahari in a similar manner. Furthermore, negative values of LAI_{model} were set to zero (no vegetation).

3.4. Comparing the Empirical Model with MODIS LAI (MOD15A2)

In order to allow for a comparison between high-resolution modeled LAI (LAI_{model}) from RapidEye and MOD15A2, the LAI_{model} was co-registered (to minimize geometric errors) and spatially aggregated (to match the 1×1 km spatial resolution of MOD15A2) [55]. The median was used for the aggregation of the LAI_{model}, due to its robustness in dealing with extreme values, which are more pronounced at high

resolution. Nevertheless, as a pixel-by-pixel comparison is hampered by locational errors and the fact that the MODIS retrieval algorithm offers a mean value of possible solutions, Yang *et al.* [56] recommend a comparison only be carried out at a multi-pixel scale.

The aggregated LAI$_{model}$ only distinguishes between vegetated and non-vegetated pixels. The pixels classified as "urban" in the MOD15A2 scene were used as a mask in the aggregated LAI$_{model}$ to exclude potentially mixed pixels, which may result from a mosaic of gardens and sealed surfaces in urban areas. The remaining non-vegetated pixels in the MOD15A2 scene were all assigned to "LAI = 0".

The consistency between the aggregated LAI$_{model}$ and MOD15A2 was tested by several metrics of model performance after Kanniah *et al.* [57]. These include:

(1). the Coefficient of determination (R^2) to specify the proportion of variance between two models explained by the predictor variable;

(2). the Root-Mean-Square-Error (RMSE), which is calculated using:

$$RMSE = \sqrt{\frac{\sum_{i=1}^{n}(x_i - y_i)^2}{n}} \tag{3}$$

where x_i is the predictor variable (*i.e.*, the aggregated LAI$_{model}$), y_i is the estimated variable (*i.e.*, MOD15A2), and n is the sample size (*i.e.*, the number of pixels);

(3). the Relative Predictive Error (RPE), which provides a directional measure from mean difference between x_i and y_i in percent and is defined as:

$$RPE = \frac{(\bar{y} - \bar{x})}{\bar{x}} \, 100 \tag{4}$$

with: $\bar{y}$, the mean of $\sum_{i=1}^{n} y_i$, and $\bar{x}$, the mean of $\sum_{i=1}^{n} x_i$;

(4). the Modified Index of Agreement (mIOA) [58]:

$$mIOA = 1 - \frac{\sum_{i=1}^{n}|x_i - y_i|}{\sum_{i=1}^{n}(|x_i - \bar{y_i}| + |y_i - \bar{y_i}|)} \tag{5}$$

The last measure provides a dimensionless index value, where 0 would indicate no fit and 1 would indicate a perfect fit between the models. In comparison to the original IOA (as used in [57]), mIOA has been shown to be more robust concerning errors introduced by outliers [59].

4. Results

4.1. Field Data

A total of 13 different vegetated FLUs were identified in the field following Mueller-Dombois & Ellenberg [39]. Several main FLUs were extended in terms of species composition (e.g., dominance of a certain species) and terrain position (*cf.* Table 2). Terrain position clearly affects species composition, as it reflects edaphic properties, such as soil salinity. Thus, low land grasslands ("*grassland tufts*", "*seasonally flooded grassland*", and "*Rennera limnophila forbs*") are often characterized by salt-tolerant species, such as *Sporobolus iocladus*, *Leptochloa fusca*, *Rennera limnophila*, or *Willkommia sarmentosa* (Table 2). In general, lower elevation FLUs show a tendency towards lower total plant cover, which may partly be attributed to recurring seasonal flooding. However, selective grazing likely alters this situation significantly and, thus, explains the wide range of plant cover in these FLUs. A potential influence of

selective grazing in grasslands at higher elevation could be indicated by the dominance of non-palatable species, such as *Aristida stipoides* and *Odyssea paucinervis*. In contrast, increasing plant cover as a function of elevation could also result from the contribution of shrub and tree strata, which are almost exclusively related to middle and top terrain position in the data.

Table 2. Overview of the *in situ* FLUs, their characteristics, and sample size ("No. of ESUs").

| FLU	Description	Characteristic Species	Total Plant Cover (%)	Predominant Terrain Position	No. of ESUs
open woodland	tree cover (>5 m) >30% or trees are dominant	*H. petersiana*	30–90	middle-top	9
wooded shrub land	shrub cover >30%	*Acacia arenaria, Acacia hebeclada tr.*	50–60	top	8
P.-L. leubnitziae shrub land	shrub cover >30%	*Pechuel-Loschea leubnitziae*	40–70	top	8
C. mopane shrub land	shrub cover >30%	*C. mopane*	40–70	middle-top	8
grassland tufts	grassland at low elevation, tuft forming species	*S. iocladus, Eragrostis lehmanniana*	10–40	bottom-middle	7
grassland medium	grassland at medium elevation	*A. stipoides, W. sarmentosa*	5–30	middle	11
grassland high	grassland at high elevation	*A. stipoides, O. paucinervis*	40–70	top	8
shrub-wooded grassland	grassland with shrub cover <30%	*A. stipoides, O. paucinervis, A arenaria, A. hebeclada tr.*	20–80	middle-top	11
P.-L. leubnitziae grassland	grassland with shrub cover <30%	*A. stipoides, O. paucinervis, P-L. leubnitziae*	20–50	top	7
seasonally flooded grassland	grassland in minor depressions, tall-growing species *vs.* intense grazing	*L. fusca, S. iocladus, Elytrophorus globularis*	10–90	bottom-middle	16
R. limnophila forbs	*R. limnophila* dominant	*R. limnophila*	10–20	bottom-middle	8
agricultural land	remains of *Pennisetum glaucum*	-	10	top	4
wetland	co-existence of vegetation, water surface and bare soil	-	40–60	bottom-middle	4

4.2. In Situ LAI (LAI$_{2200}$)

Due to the sparse vegetation present at the time of the sampling, the overall mean LAI$_{2200}$ was 0.28, with a standard error of LAI$_{2200}$ (SEL) of ±0.05 (n = 109). A median of 0.21 indicates a skewness of distribution towards lower values of LAI$_{2200}$ (*cf.* Table 3). For the two classes of green vegetation (n = 17), mean LAI$_{2200}$ was 0.47, with SEL ±0.1, which appears to be noticeably higher than the overall average, though the smaller sample size might be responsible for the increase. At the same time, Apparent Clumping Factors (ACF) for the green vegetation samples are lower as compared to the overall sample.

Accordingly, the difference between LAI_{2200} and effective LAI (LAI_{eff}) increases. Lower ACFs appear to be reasonable for these classes, as the overall sample largely consists of grassland sites (68 out of 109 sites). Hereby, the spatial distribution of foliage elements in grassland sites can be assumed to be more regular on site scale as compared to shrub lands.

Table 3. Descriptive statistics of *in situ* LAI (LAI_{2200}) and associated parameters (SEL, ACF, number of samples per site and LAI_{eff}) for all sites (n = 109) and the sites of green vegetation only (n = 17). Note that LAI_{eff} was calculated by multiplying LAI_{2200} with the respective ACF.

		LAI_{2200}	SEL	ACF	No. of Samples	LAI_{eff}
Overall (n = 109)	*Mean*	0.28	0.05	0.90	19	0.24
	Min.	0.01	0.00	0.63	14	0.01
	Max.	2.09	0.26	0.99	33	1.65
	Median	0.21	0.04	0.93	19	0.20
Green vegetation only (n = 17)	*Mean*	0.47	0.10	0.83	18	0.37
	Min.	0.22	0.04	0.66	15	0.20
	Max.	1.14	0.26	0.94	25	0.75
	Median	0.44	0.09	0.87	18	0.33
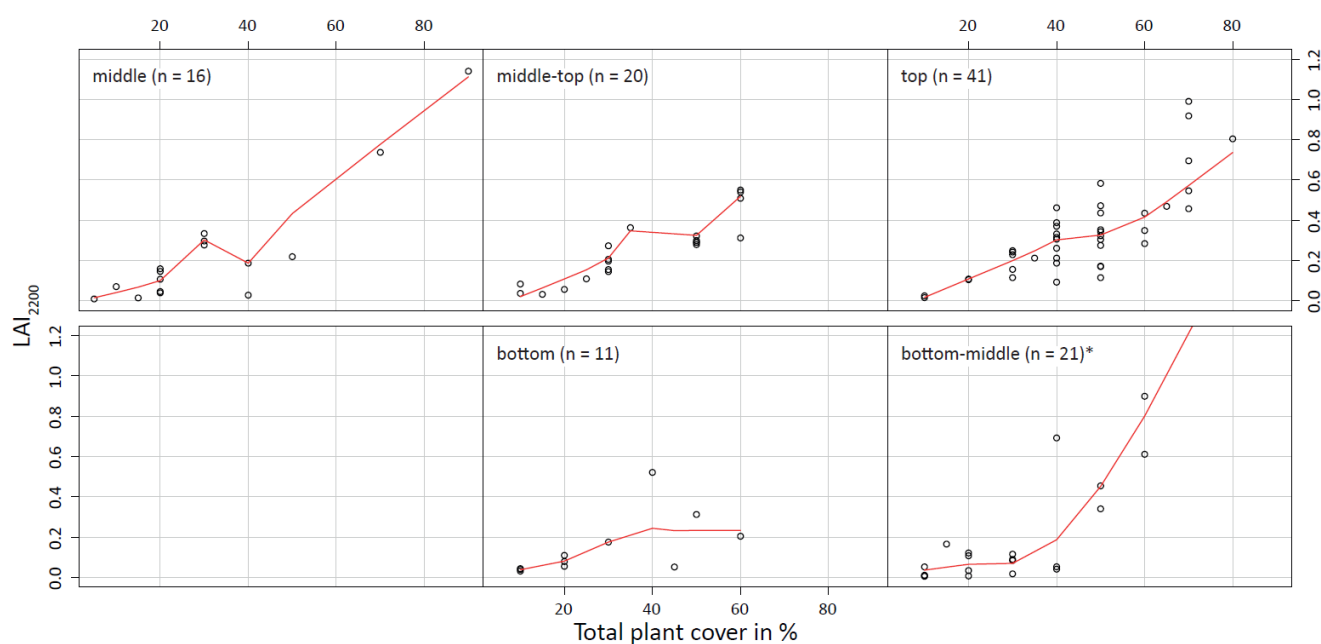
Figure 4. Conditional plots for LAI_{2200} and estimated total plant cover in %, per terrain position class. The black circles denote the samples from an ESU, the red lines show the respective LOESS smoothing lines (NOTE: the "bottom-middle"-plot only shows 20 from 21 samples due to presentation purposes).

The dependence of vegetation in the region on elevation and livestock grazing, as hypothesized in Section 4.1, is also found in the LAI_{2200} values, which generally correlate quite well with the total plant cover estimation ($R^2 = 0.61$; not depicted). Changes in these patterns determined by elevation may arise from grazing (e.g., the maximum LAI_{2200} (= 2.09) was measured at a fenced grassland site at a lower elevation). The conditional plots shown in Figure 4 mainly confirm that increasing terrain position (*i.e.*,

an increase in elevation) seems to result in higher total plant cover and LAI_{2200}. As is illustrated by the LOESS (Locally Weighted Scatterplot Smoothing) line, a near-linear trend between LAI_{2200} and total plant cover is found for higher elevated FLUs. However, this relationship is partly perturbed by fencing and species of little grazing value in FLUs of bottom to middle elevation.

4.3. Empirical-Statistical Modeling

The relationships found for the *in situ* green vegetation samples and SVIs revealed mostly moderate correlations (Table 4). This was also true for the experimental SVIs – meaning that, for this study, no advancements were achieved with the use of the RapidEye RE band. The NDVI and similar indices also provided unsatisfactory results as shown in other regions with spares vegetation (e.g., [60]). However, a sophisticated relationship between the green vegetation LAI_{2200} samples and the DVI was found ($R^2 = 0.71$). The use of a linear model seemed to be best practice as the green vegetation LAI_{2200} samples generally had low values that only covered a range of about 0.92 (*cf.* Table 3). Thus, with the LAI_{2200} serving as the explaining variable for the DVI, a linear model could be established (*cf.* Figure 5) with the transfer function:

$$LAI_{model} = \frac{DVI}{0.09} - 0.102. \tag{6}$$

Table 4. Correlations between LAI_{2200} and SVIs from linear regression.

SVI	SR	SR$_{NIR/RE}$	SR$_{RE/R}$	DVI	NDVI	NDVI$_{NIR/RE}$	NDVI$_{RE/R}$	TVI	EVI	SAVI
R^2	0.48 *	0.55 *	0.37 *	0.71 *	0.49 *	0.56 *	0.36 **	0.49 *	0.32 **	0.57 *

NOTE: * Significance (2-tailed) $p < 0.01$; ** Significance (2-tailed) $p < 0.05$
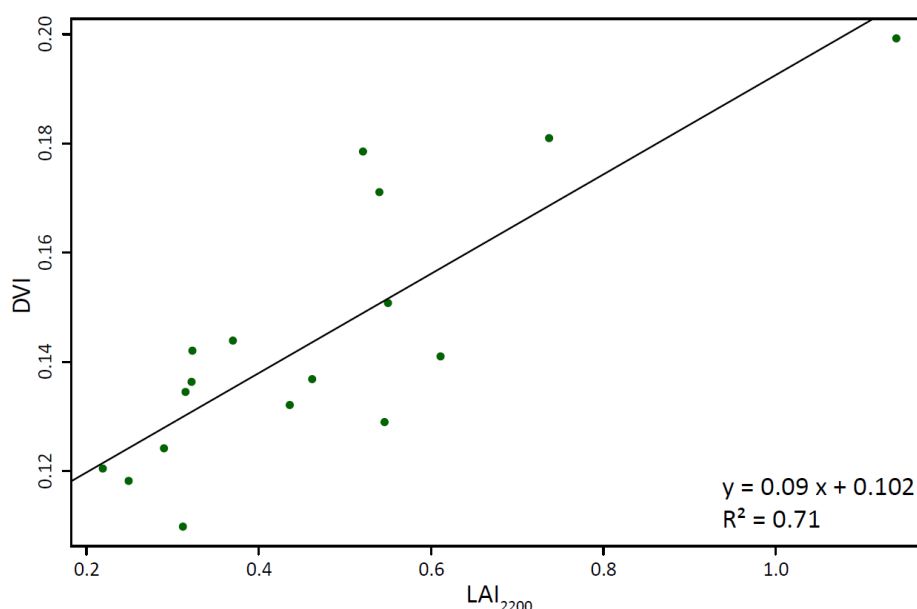
Figure 5. Bivariate plots of *in situ* LAI_{2200} and DVI derived from RapidEye imagery. The linear regression model ($R^2 = 0.71$) is indicated by the solid line, whereas green points represent samples of the classes "C. mopane shrub land" and "open woodland" (n = 17). Note the different origins of axes in the figure.

The mean of LAI$_{model}$ was 0.57 (± 0.37). As can be seen from Figure 6a, larger areas of high LAI, *i.e.*, dense vegetation, were found at the western and north-eastern edges of the study area, whereas the highest LAI (11.85) was located within an irrigated park like area in the urban area of Oshakati. The central regions, where the test sites and the 17 sites used for the model were located, mainly consist of grasslands. Thus, they are characterized by lower LAIs. Extensive non-vegetated areas were found in southern and south-eastern parts of the region. As already observed for the field data, the vegetation density is related to the topographic position.

(a) High-resolution LAI$_{model}$
(mean = 0.57 (± 0.37), max. = 11.85)

(b) Aggregated LAI$_{model}$
(mean = 0.55 (± 0.23), max. = 1.3)

(c) MODIS LAI (MOD15A2)
(mean = 0.2 (± 0.11), max. = 0.5)

(d) Differences between the LAI models
(mean = 0.34 (± 0.2), max. = 1.1, min. = -0.3)
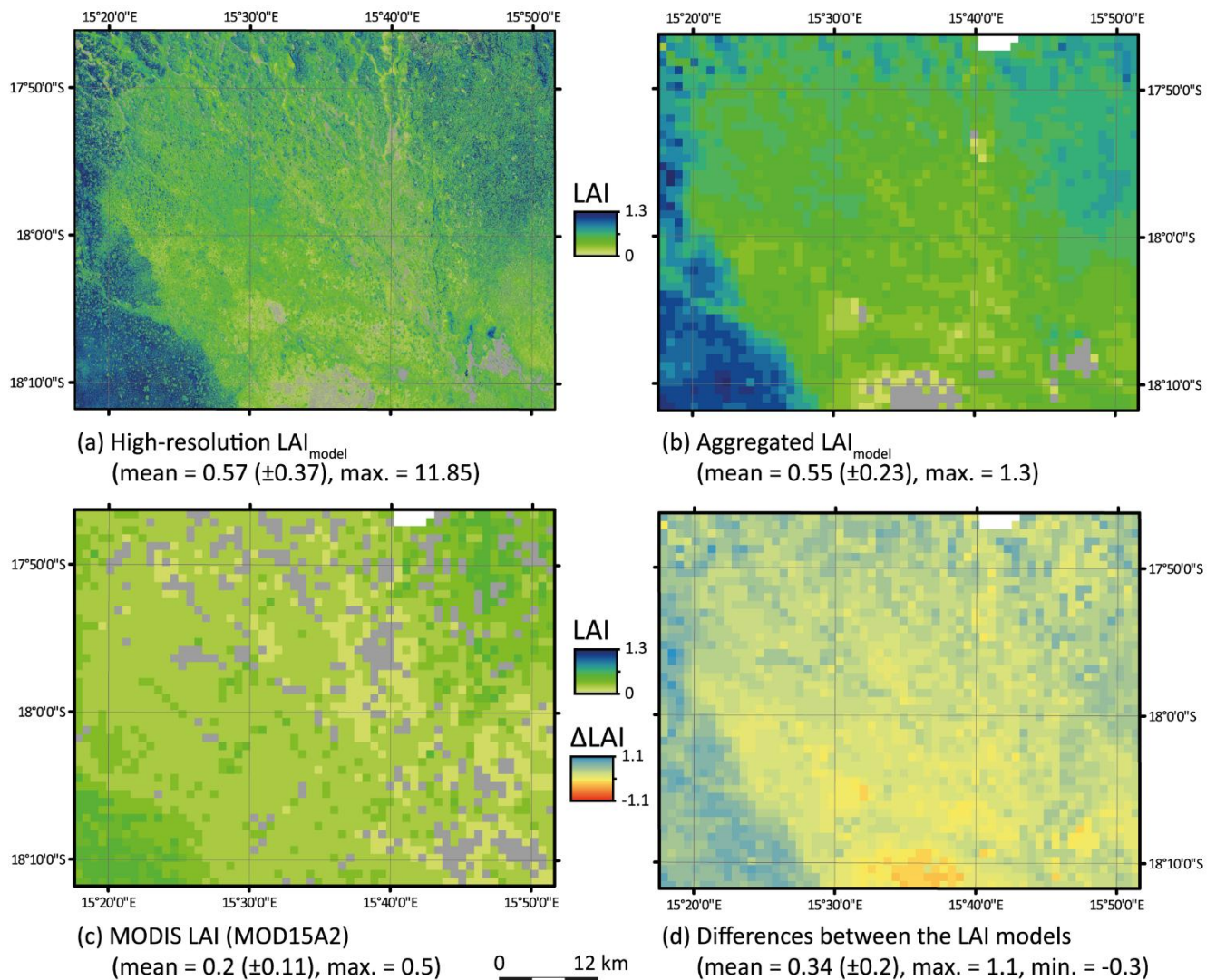
Figure 6. LAI maps of the study region: (**a**) High-resolution map of LAI$_{model}$ (5 $\times$ 5 m) based on the transfer function given in Equation (6). For cartographic reasons, no differentiation for pixels with a LAI$_{model}$ > 1.3 was made. (**b**) Aggregated map of the LAI$_{model}$. (**c**) 8-day mean MODIS LAI (MOD15A2) map (spatial resolution: 1 $\times$ 1 km). (**d**) Absolute difference between (**b**) and (**c**), where positive values indicate the aggregated LAI$_{model}$ to exceed MOD15A2, and vice versa. (NOTE: For (**b**) and (**d**), urban areas, as classified by (**c**), were a priori excluded from processing).

4.4. Comparison of the High-Resolution LAI$_{model}$ with MOD15A2

The aggregation of the high-resolution LAI$_{model}$ to the resolution of MOD15A2 (1 km) reduced the effects of spatial heterogeneity and the influence of extreme values; the maximum LAI$_{model}$ pixel value decreased from 11.85 in the high-resolution model to 1.3 at moderate resolution (aggregated LAI$_{model}$). However, as illustrated by Figure 6b, the spatial patterns of LAI are preserved, which is further expressed by a similar mean with a moderate variance, which decreased by 0.02 to 0.55.

The MOD15A2 scene used here, generally points to a more uniformly distributed LAI in regions, which can be attributed to the more coarse initial spatial resolution of MOD15A2. Though the spatial patterns of LAI coincidence at a multi-pixel scale, only moderate consistency was found regarding the magnitude of LAI between the two models. This is especially true for areas with a higher LAI (e.g., western margin of the study area), where the variation between the aggregated LAI$_{model}$ and MOD15A2 often exceeds 0.5 LAI units (max. = 1) (*cf.* Figure 6d). For the central and southern parts of the study area, the offset is lower (often around 0.1–0.3 units LAI). Though the mean of the aggregated LAI$_{model}$ is higher than MOD15A2, certain areas in the central south also show an underestimation up to 0.3 units LAI.

One major source of inconsistency between the aggregated LAI$_{model}$ and MOD15A2 is related to the differing spatial distribution of non-vegetated pixels, which can already be recognized through visual interpretation (grey in Figure 6b,c). Further confirmation comes from the calculated measures of model performance (*cf.* Table 5): whereas RMSE and RPE only show minor improvements, the R^2 from linear regression and the mIOA reveal a distinct increase in model fit if all non-vegetated pixels from the MOD15A2 scene are excluded.

Table 5. Comparing the aggregated LAI$_{model}$ and MODIS LAI. Measures of model performance for all pixels (upper row; n = 2811) and vegetated pixels only in the MOD15A2 scene (lower row; n = 2448): the linear model equation and the corresponding Coefficient of Determination (R^2), Root-Mean-Square Error (RMSE), Relative Predictive Error (RPE) and the Modified Index of Agreement (mIOA).

x	Pixels Valid (n)	Linear Model	R^2	RMSE	RPE	mIOA
MODIS LAI	2811	y = 0.8463x + 0.371	0.182	0.40	−62.97%	0.13
MODIS LAI > 0	2448	y = 1.3396x + 0.2521	0.293	0.39	−59.18%	0.42

5. Discussion

5.1. Sampling

A critical issue for retrieving *in situ* environmental parameters is the determination of a suitable sampling strategy [61,62]. The preferential-stratified approach, as applied here, risks the inclusion of circular reasoning. The data retrieved might merely reflect the environmental criteria used for stratification [63]. On the other hand, this strategy is highly effective for the sampling of the maximum diversity of FLUs with a relatively small number of samples. In contrast, purely random approaches have the potential to show limited representativeness (oversampling of frequently occurring FLUs, undersampling of rare or spatially restricted FLUs). Furthermore, their common perception as being statistically independent is initially impaired by a general spatial auto-correlation of vegetation [63].

5.2. In Situ LAI

Compared to other biomes, savannas are underrepresented in studies focusing on the indirect sampling of LAI [64], where even fewer deal with dry season LAI. For example, Boulain *et al.* [10] investigated a shrub land fallow in Western Niger (MAP = 479 mm) with the annual minima of LAI ranging between 0.1 and 0.2. From Southern Africa, Privette *et al.* [21] report a mean dry season LAI of 0.8 in Zambia (MAP = 950 mm), whereas a mean dry season LAI of 0.79 (±0.13) was found in several Miombo woodland sites in Northern Mozambique (MAP = 900 mm) [65]. Within the Kalahari Transect [64], two shrub land sites located in Tsane (MAP = 350 mm) and Okwa (MAP = 424 mm) in Botswana were sampled during a drought period within the growing season. Here, LAI ranged between 0.51 and 0.83 in Tsane and between 0.19 and 1.75 in Okwa. In a study from Australia [66], dry season LAI means ranged from 0.1 to 2.1 along an precipitation gradient from below 400 mm/yr to above 1200 mm/yr. Therefore, a mean LAI_{2200} of 0.28 (±0.05) in our study region in Northern-Central Namibia with a MAP between 400 and 500 mm is well in the range of the other studies carried out in dry-season savanna environments.

Ryu *et al.* [27] attribute the great challenge of accurately deriving LAI from indirect methods in savannas to the quantification of a spatially representative element clumping index (Ω). The ACF, as provided with the estimates from the Li-Cor LAI-2200 instrument, gives an approximate measure of clumping. Instruments measuring gap-size distribution, such as the "Tracing Radiation and Canopy Architecture (TRAC)"-device or Digital Hemispherical Photography (DHP), would provide a more correct derivation of Ω [27]. Another possibility to account for the non-random distribution of vegetation elements is the *post hoc* incorporation of an external, satellite-derived Ω (e.g., from [67]). However, the ACF values, as calculated with the instrument used here, seem to produce reasonable results. Specifically, "Open woodland" appears to occupy the lowest ACF, while grasslands mostly account for the highest ACFs, *i.e.*, relatively little clumping is observed (not shown). The same is confirmed by Ryu *et al.* [68], who conclude that the ACF gives a good approximation of clumping at site level, whereas the additional usage of an external Ω would possibly result in an "overcorrection" of foliage clumping with this device.

The contribution of non-photosynthetic canopy elements, woody area index (WAI), to estimates of LAI is the subject of an on-going controversy [16]. Owing to the fact that woody components are inherently spatially auto-correlated with the photosynthetic features of a canopy, the contribution of WAI to LAI_{2200} is likely to decrease as the growing season proceeds. For grasses and non-deciduous species, variations in foliage shape (e.g., leaf roll up) and inclination may introduce biases, not only for the contribution of WAI, but also for LAI determination itself. Phenology may further affect optically-derived LAI estimates, as with senescent leaves the transmittance of radiation increases and, hence, LAI is underestimated [6].

5.3. Empirical-Statistical Modeling

High-resolution satellite images, such as the RapidEye scene used in this study, enable the proper mapping of landscape heterogeneity and spatially distinct phenomena. In accordance with Ehammer *et al.* [54], who report no improvement of LAI and FPAR modeling from SVIs incorporating RapidEye's RE band in a Central-Asian agro-ecosystem, the correlations of SVIs using the RE band with LAI_{2200} were only

moderate in this study (*cf.* Table 4). The insignificance of the RE band for the detection of LAI found here may be attributed to the broad range covered by this band (40 nm). Another reason could be the poorly distinctive inflexion point of the RE band and, thus, a nearly linear slope for vegetation reflectance between R and NIR bands.

For the creation of the high-resolution map of LAI (LAI$_{model}$), a linear transfer function was established as the highest agreement for all SVIs tested was found between LAI$_{2200}$ and the DVI (*cf.* Table 4). The DVI has often been found to be linearly related with LAI [43,69]. As mentioned earlier, an *in situ* quantification of WAI could not be performed. The adopted value of 0.35 for WAI was subtracted from LAI$_{model}$ with the aim of approximately transferring the empirically calibrated LAI to estimates of "real" LAI. As the latter measure is given by MOD15A2, this processing step was the best practice possible to carry out a comparison, being aware that such approaches simplify the diverse nature of WAI.

Qi *et al.* [20] point out that also the general relationship between a given SVI and LAI may differ substantially with the vegetation types considered. A major limitation of the applied transfer function is that only 17 of all 109 sample sites contained mainly green vegetation at this time of the year. Grasslands, which cover large parts of the study area, could not be included in the model calibration. Nevertheless, the full range of LAI was covered by the 17 samples, which are representative for the region. The excluded samples had mostly very low LAIs. Including them would have caused a concentration of low values in the regression model shown in Figure 5.

As the signal detected by a given SVI refers to the amount of green vegetation [49], senescent vegetation would only have been indirectly detected by the SVI as a function of reduced soil background reflectance. In general, the noise introduced by the underlying soil and litter is regarded as a major challenge associated with SVIs [69–71]. Litter and standing senescent vegetation together with bright and dry sandy soils in the study area may serve as a severe source of error for the detected spectral signals. Accordingly, in sparsely vegetated ecosystems, soil background reflectance leads to an overestimation of the SVI and, hence, of the derived biophysical variables as well [70]. To date, several approaches have been developed to account for soil background reflectance. A simple example is the SAVI. However, the SAVI achieved only moderate performance in this study (*cf.* Table 4). Other approaches to discriminate senescent vegetation and litter make use of the Short-Wave and Mid-Wave Infrared spectra (SWIR, MWIR). Marsett *et al.* [72] introduced the Soil Adjusted Total Vegetation Index (SATVI), while other approaches used a combination of NDVI and the Cellulose Absorption Index (CAI) to discriminate green and senescent vegetation from bare soil [73]. However, SWIR and MWIR spectra are not covered by the RapidEye bands.

5.4. Comparison with MOD15A2

In general, the conclusions drawn from a comparison between *in situ* LAI and satellite-derived LAI products often lack spatial coverage due to the discrete nature of *in situ* measurements. Scholes *et al.* [64] compared *in situ* LAI estimates with a respective MOD15A2 scene concluding that MOD15A2 tended towards underestimation with increasing aridity as compared to AccuPAR ceptometer estimates. Privette *et al.* [21] found that MOD15A2 tended towards overestimation for dry sites and the contrary for wet sites. Fensholt *et al.* [23] report that MOD15A2 overestimated LAI, especially during the dry

season in Senegal. Tian *et al.* [22] again, find underestimations of LAI using MOD15A2 in savanna ecosystems, which they generally attribute to increased soil background contamination with lower spatial image resolution as well as the heterogeneity of these ecosystems.

The approach followed in this study was to model *in situ* LAI_{2200} with a low level of generalization, *i.e.*, using high resolution data. The spatial aggregation of this LAI_{model} enabled a comparison with MOD15A2 for the entire study area. However, only a moderate agreement between these two models was found (*cf.* Table 5). For large parts of the study area, overestimation was found, which often exceeded the range of the standard deviation of MOD15A2 (*cf.* Figure 7a). This overestimation is in accordance with some of the above-mentioned studies. However, certain areas in the south of our study area show an opposite trend (*cf.* Figure 6d). The results presented here and the conclusions drawn from the above-mentioned studies highlight the inconsistencies associated with LAI estimations in savanna ecosystems.

(a) Standard Deviation of MODIS LAI (MOD15A2)

(b) Monthly MODIS burned Area (MCD45A1)
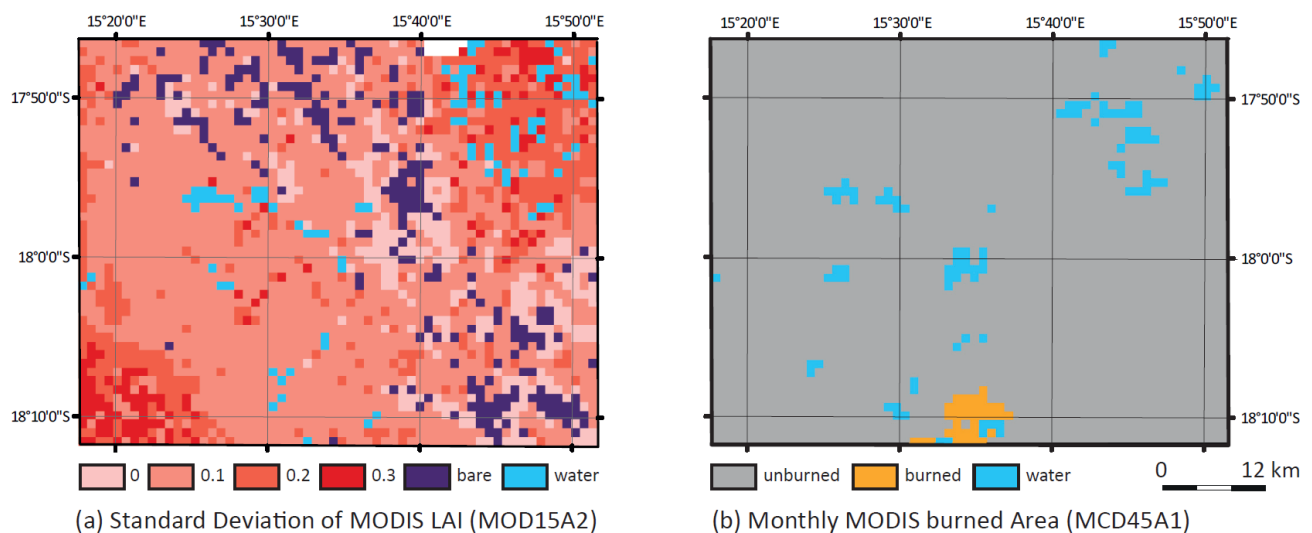
Figure 7. (**a**) Standard deviation of MODIS LAI (MOD15A2) and non-vegetated pixels (grey in Figure 6c) separated into desert (black) and water (blue). (**b**) Monthly MODIS Burned Area (MCD45A1) product from September 2010.

As the main MOD15A2 algorithm relies on a land cover map (*i.e.*, the MCD12Q1 product) for the structural canopy attributes, one critical issue for the performance of MOD15A2 is the correct biome allocation [24]. Fang *et al.* [74] compared global datasets of the MOD15A2 and MCD12Q1 for the time span from 2003 to 2009, concluding that biome misclassification and, thus, LAI overestimation would be highest for savannas, again in accordance with our results. For our study region, biomes were correctly assigned in MCD12Q1 ("annual broadleaf vegetation" and "annual grass vegetation"; not depicted). However, the classification of non-vegetated pixels in MOD15A2 apparently affected the model performance negatively (*cf.* Table 5). Differing initial spatial, temporal, and spectral resolutions as well as the aggregation process can be hypothesized to ultimately result in an inconsistent distribution of non-vegetated pixels between high-resolution models and the MOD15A2 product. Non-vegetated pixels, as assigned by MCD12Q1, are *a priori* excluded from computation of MOD15A2 [75]. For the study area, the temporal resolution of MCD12Q1, which represents the annual average of the preceding

year, could lead to errors due to sparse vegetation cover as well as intra-annually changing land cover resulting from seasonal flooding, drought or fire. These effects are illustrated through the varying distribution of water bodies from MCD12Q1 (*cf.* Figure 7a) and the MODIS Burned Area Product (MCD45A1; *cf.* Figure 7b). For the monthly MCD45A1, water bodies are derived from daily MODIS surface spectral reflectances (MOD09) by applying thresholds for NDVI (<0.1), band 7 (<0.04) and/or the quality assessment (QA) table [76].

Furthermore, our LAI model appears to show sensitivity to ecological disturbance from fire. The MCD45A1 product identifies the burning of a region, located in the central-southern part of the study area (*cf.* Figure 7b), to have occurred on Sep 23 and 24, 2010. Although no quantitative estimate of the intensity of these fires can be drawn, its spatial extent (34 pixels or km^2) is not negligible. However, this vegetation anomaly is not detected in the MOD15A2 scene. Though the causality of this issue needs a further examination, it may point to a potential for optimization of MOD15A2 by the incorporation of vegetation anomalies derived from MCD45A1.

6. Conclusions

The study presented here used field and remote sensing data to assess dry-season vegetation patterns, thereby focusing on LAI in a savanna ecosystem located in Northern-Central Namibia. In order to expand pattern identification from a point to a regional scale, we used an empirical-statistical approach to model LAI. Due to senescent vegetation, a constrained number of LAI$_{2200}$ samples were used in this process. Nevertheless, a sophisticated relationship was retrieved between green-vegetation LAI$_{2200}$ and the DVI derived from RapidEye reflectances. The red-edge channel of the RapidEye sensor did not improve modeling results in the dry season with predominantly senescent vegetation. However, with the high resolution it is possible to record the spatial heterogeneity of savanna ecosystems. Sensors with a resolution of RapidEye and bands in the MWIR are expected to yield in higher accuracy of dry-season LAI estimations. Further improvements are possible for the field measurements [44] on which the high-resolution models are based.

A comparison with MODIS LAI (MOD15A2) revealed several inconsistencies. These included a mean negative offset of MOD15A2 and its insensitivity to vegetation anomalies, induced by disturbance like fire. In general, the results of our study are in accordance with other studies carried out under similar conditions and comparable phenological stages. The given differences, mainly overestimations, to the MOD15A2 product are tolerable, especially because the general spatial patterns are consistent in the three methods, field measurement, high-resolution model and MOD15A2.

Our study is a contribution to the validation of standard LAI products in an ecological setup, which is underrepresented in similar studies, especially during the dry season. Despite the discussed variation of the measured and modeled LAI in such reason the overall results prove to be consistent and the standard MODIS LAI product (MOD15A2) is robust.

Acknowledgments

Author Contributions

Both authors contributed significantly to this manuscript. Cyrus Samimi conceived and designed the research. Both authors designed the sampling campaign. Manuel J. Mayr collected the *in situ* data. Manuel J. Mayr processed and analyzed *in situ* and remote sensing data. Both authors lively discussed the results and their implications. Manuel J. Mayr wrote the paper.

Conflicts of Interest

The authors declare no conflict of interest.

References

1. Seghieri, J.; Floret, C.; Pontanier, R. Plant phenology in relation to water availability: Herbaceous and woody species in the savannas of northern Cameroon. *J. Trop. Ecol.* **1995**, *11*, 237–254.
2. Scholes, R.J.; Archer, S.R. Tree-grass interactions in Savannas. *Ann. Rev. Ecol. Syst.* **1997**, *28*, 517–544.
3. Wagenseil, H.; Samimi, C. Woody vegetation cover in Namibian savannahs: A modelling approach based on remote sensing. *Erdkunde* **2007**, *61*, 325–334.
4. Barclay, H.J. Conversion of total leaf area to projected leaf area in lodgepole pine and Douglas-fir. *Tree Physiol.* **1998**, *18*, 185–193.
5. Weiss, M.; Baret, F.; Smith, G.J.; Jonckheere, I.; Coppin, P. Review of methods for *in situ* leaf area index (LAI) determination Part II. Estimation of LAI, errors and sampling. *Agric. For. Meteorol.* **2004**, *121*, 37–53.
6. Garrigues, S.; Shabanov, N.V.; Swanson, K.; Morisette, J.T.; Baret, F.; Myneni, R.B. Intercomparison and sensitivity analysis of Leaf Area Index retrievals from LAI-2000, AccuPAR, and digital hemispherical photography over croplands. *Agric. For. Meteorol.* **2008**, *148*, 1193–1209.
7. Liu, J.; Chen, J.M.; Cihlar, J.; Park, W.M. A process-based boreal ecosystem productivity simulator using remote sensing inputs. *Remote Sens. Environ.* **1997**, *62*, 158–175.
8. Novick, K.A.; Stoy, P.C.; Katul, G.G.; Ellsworth, D.S.; Siqueira, M.B.S.; Juang, J.; Oren, R. Carbon dioxide and water vapor exchange in a warm temperate grassland. *Oecologia* **2004**, *138*, 259–274.
9. Chen, J.M.; Chen, X.; Ju, W.; Geng, X. Distributed hydrological model for mapping evapotranspiration using remote sensing inputs. *J. Hydrol.* **2005**, *305*, 15–39.
10. Boulain, N.; Cappelaere, B.; Ramier, D.; Issoufou, H.B.A.; Halilou, O.; Seghieri, J.; Guillemin, F.; Oï, M.; Gignoux, J.; Timouk, F. Towards an understanding of coupled physical and biological processes in the cultivated Sahel-2. Vegetation and carbon dynamics. *J. Hydrol.* **2009**, *375*, 190–203.

11. Kraus, T. Ground-based Validation of the MODIS Leaf Area Index Product for East African Rain Forest Ecosystems. Ph.D. Thesis, Friedrich-Alexander University, Erlangen-Nuremberg, Germany, 10 October 2008.

12. Bréda, N.J.J. Ground-based measurements of leaf area index: A review of methods, instruments and current controversies. *Journal Exp. Bot.* **2003**, *54*, 2403–2417.

13. Jonckheere, I.; Fleck, S.; Nackaerts, K.; Muys, B.; Coppin, P.; Weiss, M.; Baret, F. Review of methods for *in situ* leaf area index determination Part I. Theories, sensors and hemispherical photography. *Agric. For. Meteorol.* **2004**, *121*, 19–35.

14. Welles, J.M.; Cohen, S. Canopy structure measurement by gap fraction analysis using commercial instrumentation. *J. Exp. Bot.* **1996**, *47*, 1335–1342.

15. Gower, S.T.; Kucharik, C.J.; Norman, J.M. Direct and indirect estimation of leaf area index, f(APAR), and net primary production of terrestrial ecosystems. *Remote Sens. Environ.* **1999**, *70*, 29–51.

16. Van Gardingen, P.R.; Jackson, G.E.; Hernandez-Daumas, S.; Russell, G.; Sharp, L. Leaf area index estimates obtained for clumped canopies using hemispherical photography. *Agric. For. Meteorol.* **1999**, *94*, 243–257.

17. Chen, J.M.; Black, T.A. Defining leaf area index for non-flat leaves. *Plant. Cell. Environ.* **1992**, *15*, 421–429.

18. Asner, G.P.; Scurlock, J.M.O.; Hicke, J.A. Global synthesis of leaf area index observations: Implications for ecological and remote sensing studies. *Glob. Ecol. Biogeogr.* **2003**, *12*, 191–205.

19. Dorigo, W.A.; Zurita-Milla, R.; de Wit, A.J.W.; Brazile, J.; Singh, R.; Schaepman, M.E. A review on reflective remote sensing and data assimilation techniques for enhanced agroecosystem modeling. *Int. J. Appl. Earth Obs. Geoinf.* **2007**, *9*, 165–193.

20. Qi, J.; Kerr, Y.H.; Moran, M.S.; Weltz, M.; Huete, A.R.; Sorooshian, S.; Bryant, R. Leaf area index estimates using remotely sensed data and BRDF models in a semiarid region. *Remote Sens. Environ.* **2000**, *73*, 18–30.

21. Privette, J.L.; Myneni, R.B.; Knyazikhin, Y.; Mukelabai, M.; Roberts, G.; Tian, Y.; Wang, Y.; Leblanc, S.G. Early spatial and temporal validation of MODIS LAI product in the Southern Africa Kalahari. *Remote Sens. Environ.* **2002**, *83*, 232–243.

22. Tian, Y.; Woodcock, C.E.; Wang, Y.; Privette, J.L.; Shabanov, N.V.; Zhou, L.; Zhang, Y.; Buermann, W.; Dong, J.; Veikkanen, B.; *et al.* Multiscale analysis and validation of the MODIS LAI product I. Uncertainty assessment. *Remote Sens. Environ.* **2002**, *83*, 414–430.

23. Fensholt, R.; Sandholt, I.; Rasmussen, M.S. Evaluation of MODIS LAI, fAPAR and the relation between fAPAR and NDVI in a semi-arid environment using *in situ* measurements. *Remote Sens. Environ.* **2004**, *91*, 490–507.

24. Hill, M.J.; Senarath, U.; Lee, A.; Zeppel, M.; Nightingale, J.M.; Williams, R.J.; McVicar, T.R. Assessment of the MODIS LAI product for Australian ecosystems. *Remote Sens. Environ.* **2006**, *101*, 495–518.

25. Kraus, T.; Schmidt, M.; Dech, S.W.; Samimi, C. The potential of optical high resolution data for the assessment of leaf area index in East African rainforest ecosystems. *Int. J. Remote Sens.* **2009**, *30*, 5039–5059.

26. Serbin, S.P.; Ahl, D.E.; Gower, S.T. Spatial and temporal validation of the MODIS LAI and FPAR products across a boreal forest wildfire chronosequence. *Remote Sens. Environ.* **2013**, *133*, 71–84.

27. Ryu, Y.; Sonnentag, O.; Nilson, T.; Vargas, R.; Kobayashi, H.; Wenk, R.; Baldocchi, D.D. How to quantify tree leaf area index in an open savanna ecosystem: A multi-instrument and multi-model approach. *Agric. For. Meteorol.* **2010**, *150*, 63–76.

28. Okin, G.S. The contribution of brown vegetation to vegetation dynamics. *Ecology* **2010**, *91*, 743–755.

29. Bond, W.J.; van Wilgen, B.W. *Fire and Plants*, 1st ed.; Chapman & Hall: London, UK, 1996.

30. Mendelsohn, J.M.; El Obeid, S.; Roberts, C. *A Profile of North-Central Namibia*; Gamsberg Macmillan Publishers: Windhoek, Namibia, 2000.

31. Kluge, T.; Liehr, S.; Lux, A.; Moser, P.; Niemann, S.; Umlauf, N.; Urban, W. IWRM concept for the Cuvelai Basin in northern Namibia. *Phys. Chem. Earth* **2008**, *33*, 48–55.

32. Mendelsohn, J.M.; Jarvis, A.; Roberts, C.; Robertson, T. *Atlas of Namibia*: *A Portrait of the Land and Its People*; David Philip: Cape Town, South Africa, 2002.

33. RapidEye AG. *RapidEye Satellite Imagery Product Specifications. Version 3.2.*; RapidEye AG: Brandenburg An der Havel, Germany, 2011.

34. Song, C.; Woodcock, C.E.; Seto, K.C.; Lenney, M.P.; Macomber, S.A. Classification and change detection using Landsat TM data: When and how to correct atmospheric effects? *Remote Sens. Environ.* **2001**, *75*, 230–244.

35. Mather, P.M.; Koch, M. *Computer Processing of Remotely-Sensed Images*: *An. Introduction*, 4th ed.; Wiley-Blackwell: Chichester, UK 2011.

36. Yang, W.; Shabanov, N.V.; Huang, D.; Wang, W.; Dickinson, R.E.; Nemani, R.R.; Knyazikhin, Y.; Myneni, R.B. Analysis of leaf area index products from combination of MODIS Terra and Aqua data. *Remote Sens. Environ.* **2006**, *104*, 297–312.

37. Shabanov, N.V.; Huang, D.; Yang, W.; Tan, B.; Knyazikhin, Y.; Myneni, R.B.; Ahl, D.E.; Gower, S.T.; Huete, A.R.; Arag ão, L.E.O.C.; *et al.* Analysis and optimization of the MODIS leaf area index algorithm retrievals over broadleaf forests. *IEEE Trans. Geosci. Remote Sens.* **2005**, *43*, 1855–1865.

38. Fang, H.; Jiang, C.; Li, W.; Wei, S.; Baret, F.; Chen, J.M.; Garcia-Haro, J.; Liang, S.; Liu, R.; Myneni, R.B.; *et al.* Characterization and intercomparison of global moderate resolution leaf area index (LAI) products: Analysis of climatologies and theoretical uncertainties. *J. Geophys. Res.: Biogeosci.* **2013**, *118*, 529–548.

39. Mueller-Dombois, D.; Ellenberg, H. *Aims and Methods of Vegetation Ecology*; John Wiley & Sons: New York, NY, USA, 1974.

40. Giladi, I.; Ziv, Y.; May, F.; Jeltsch, F. Scale-dependent determinants of plant species richness in a semi-arid fragmented agro-ecosystem. *J. Veg. Sci.* **2011**, *22*, 983–996.

41. LI-COR Inc. *LAI-2200 Plant. Canopy Analyzer Instruction Manual*; Li-Cor Inc.: Lincoln, NE, USA, 2009.

42. Nilson, T. A theoretical analysis of the frequency of gaps in plant stands. *Agr. Meteorol.* **1971**, *8*, 25–38.

43. Jones, H.G.; Vaughan, R.A. *Remote Sensing of Vegetation*: *Principles, Techniques, and Applications*; Oxford University Press: Oxford, UK and New York, NY, USA, 2010.

44. Kobayashi, H.; Ryu, Y.; Baldocchi, D.D.; Welles, J.M.; Norman, J.M. On the correct estimation of gap fraction: How to remove scattered radiation in gap fraction measurements? *Agric. For. Meteorol.* **2013**, *174–175*, 170–183.

45. White, M.A.; Asner, G.P.; Nemani, R.R.; Privette, J.L.; Running, S.W. Measuring fractional cover and leaf area index in arid ecosystems: Digital camera, radiation transmittance, and laser altimetry methods. *Remote Sens. Environ.* **2000**, *74*, 45–57.

46. Garrigues, S.; Allard, D.; Weiss, M.; Baret, F. Comparing VALERI Sampling Schemes to Better Represent High Spatial Resolution Satellite Pixel from Ground Measurements: How to Characterize an ESU. Available online: http://www.avignon.inra.fr/valeri/methodology/samplingschemes.pdf (accessed on 25 January 2015).

47. Bannari, A.; Morin, D.; Bonn, F.; Huete, A.R. A review of vegetation indices. *Remote Sens. Rev.* **1995**, *13*, 95–120.

48. Baret, F.; Guyot, G. Potentials and limits of vegetation indices for LAI and APAR assessment. *Remote Sens. Environ.* **1991**, *35*, 161–173.

49. Huete, A.R.; Justice, C.; van Leeuwen, W. MODIS Vegetation Index (MOD 13)—Algorithm Theoretical Basis Document (Version 3). Available online: http://modis.gsfc.nasa.gov/data/atbd/atbd_mod13.pdf (accessed on 25 January 2015).

50. Birth, G.S.; McVey, G.R. Measuring the color of growing turf with a reflectance spectrophotometer. *Agron. J.* **1968**, *60*, 640–643.

51. Tucker, C.J. Red and photographic infrared linear combinations for monitoring vegetation. *Remote Sens. Environ.* **1979**, *8*, 127–150.

52. Rouse, J.W., Jr.; Haas, R.H.; Deering, D.W.; Schell, J.A. Monitoring the Vernal Advancement and Retrogradiation (Green Wave Effect) of Natural Vegetation. Available online: http://ntrs.nasa.gov/archive/nasa/casi.ntrs.nasa.gov/19740004927.pdf (accessed on 10 April 2015).

53. Deering, D.W.; Haas, R.H. Using Landsat Digital Data for Estimating Green Biomass. Available online: http://ntrs.nasa.gov/archive/nasa/casi.ntrs.nasa.gov/19800024311.pdf (accessed on 25 January 2015).

54. Ehammer, A.; Fritsch, S.; Conrad, C.; Lamers, J.; Dech, S. Statistical derivation of fPAR and LAI for irrigated cotton and rice in arid Uzbekistan by combining multi-temporal RapidEye data and ground measurements. *Proc. SPIE* **2010**, *782409*, doi:10.1117/12.864796.

55. Morisette, J.T.; Baret, F.; Privette, J.L.; Myneni, R.B.; Nickeson, J.E.; Garrigues, S.; Shabanov, N.V.; Weiss, M.; Fernandes, R.A.; Leblanc, S.G.; *et al.* Validation of global moderate-resolution LAI products: A framework proposed within the CEOS land product validation subgroup. *IEEE Trans. Geosci. Remote Sens.* **2006**, *44*, 1804–1814.

56. Yang, W.; Tan, B.; Huang, D.; Rautiainen, M.; Shabanov, N.V.; Wang, Y.; Privette, J.L.; Huemmrich, K.F.; Fensholt, R.; Sandholt, I.; *et al.* MODIS leaf area index products: From validation to algorithm improvement. *IEEE Trans. Geosci. Remote Sens.* **2006**, *44*, 1885–1896.

57. Kanniah, K.D.; Beringer, J.; Hutley, L.B.; Tapper, N.J.; Zhu, X. Evaluation of Collections 4 and 5 of the MODIS Gross Primary Productivity product and algorithm improvement at a tropical savanna site in northern Australia. *Remote Sens. Environ.* **2009**, *113*, 1808–1822.

58. Willmott, C.J.; Ackleson, S.G.; Davis, R.E.; Feddema, J.J.; Klink, K.M.; Legates, D.R.; O'Donnell, J.; Rowe, C.M. Statistics for the evaluation and comparison of models. *J. Geophys. Res.* **1985**, *90*, 8995–9005.

59. Willmott, C.J.; Robeson, S.M.; Matsuura, K. A refined index of model performance. *Int. J. Climatol.* **2012**, *32*, 2088–2094.

60. Zandler, H.; Brenning, A.; Samimi, C. Quantifying dwarf shrub biomass in an arid environment: Comparing empirical methods in a high dimensional setting. *Remote Sens. Environ.* **2015**, *158*, 140–155.

61. Law, B.E.; Campbell, J.L.; Chen, J.M.; Sun, O.; Schwartz, M.; van Ingen, C.; Verma, S. Terrestrial Carbon Observations: Protocols for Vegetation Sampling and Data Submission, Report of the Global Terrestrial Observing System (GTOS). Available online: http://www.fao.org/gtos/doc/pub55.pdf (accessed on 10 April, 2015).

62. Zhang, J.; Zhang, C. Sampling and sampling strategies for environmental analysis. *Int. J. Environ. Anal. Chem.* **2012**, *92*, 466–478.

63. Roleček, J.; Chytrý, M.; Hájek, M.; Lvončík, S.; Tichý, L. Sampling design in large-scale vegetation studies: Do not sacrifice ecological thinking to statistical purism! *Folia Geobot.* **2007**, *42*, 199–208.

64. Scholes, R.J.; Frost, P.G.H.; Tian, Y. Canopy structure in savannas along a moisture gradient on Kalahari sands. *Glob. Chang. Biol.* **2004**, *10*, 292–302.

65. Ribeiro, N.S.; Saatchi, S.S.; Shugart, H.H.; Washington-Allen, R.A. Aboveground biomass and leaf area index (LAI) mapping for Niassa Reserve, northern Mozambique. *J. Geophys. Res. Biogeosci.* **2008**, *113*, doi:10.1029/2007JG000550.

66. Sea, W.B.; Choler, P.; Beringer, J.; Weinmann, R.A.; Hutley, L.B.; Leuning, R. Documenting improvement in leaf area index estimates from MODIS using hemispherical photos for Australian savannas. *Agric. For. Meteorol.* **2011**, *151*, 1453–1461.

67. Hill, M.J.; Román, M.O.; Schaaf, C.B.; Hutley, L.; Brannstrom, C.; Etter, A.; Hanan, N.P. Characterizing vegetation cover in global savannas with an annual foliage clumping index derived from the MODIS BRDF product. *Remote Sens. Environ.* **2011**, *115*, 2008–2024.

68. Ryu, Y.; Nilson, T.; Kobayashi, H.; Sonnentag, O.; Law, B.E.; Baldocchi, D.D. On the correct estimation of effective leaf area index: Does it reveal information on clumping effects? *Agric. For. Meteorol.* **2010**, *150*, 463–472.

69. Meza-Díaz, B.; Blackburn, G.A. Remote sensing of mangrove biophysical properties: Evidence from a laboratory simulation of the possible effects of background variation on spectral vegetation indices. *Int. J. Remote Sens.* **2003**, *24*, 53–73.

70. Van Leeuwen, W.; Huete, A.R. Effects of standing litter on the biophysical interpretation of plant canopies with spectral indices. *Remote Sens. Environ.* **1996**, *55*, 123–138.

71. Pinty, B.; Lavergne, T.; Widlowski, J.-L.; Gobron, N.; Verstraete, M.M. On the need to observe vegetation canopies in the near-infrared to estimate visible light absorption. *Remote Sens. Environ.* **2009**, *113*, 10–23.

72. Marsett, R.C.; Qi, J.; Heilman, P.; Biedenbender, S.H.; Watson, M.C.; Amer, S.; Weltz, M.; Goodrich, D.; Marsett, R. Remote sensing for grassland management in the arid Southwest. *Rangeland Ecol. Manage.* **2006**, *59*, 530–540.

73. Guerschman, J.P.; Hill, M.J.; Renzullo, L.J.; Barrett, D.J.; Marks, A.S.; Botha, E.J. Estimating fractional cover of photosynthetic vegetation, non-photosynthetic vegetation and bare soil in the Australian tropical savanna region upscaling the EO-1 Hyperion and MODIS sensors. *Remote Sens. Environ.* **2009**, *113*, 928–945.

74. Fang, H.; Li, W.; Myneni, R.B. The impact of potential land cover misclassification on MODIS Leaf Area Index (LAI) estimation: A statistical perspective. *Remote Sens.* **2013**, *5*, 830–844.

75. Myneni, R.B. Personal communication, Boston University, Boston, MA, USA, 2013.

76. Boschetti, L.; Roy, D.; Hoffmann, A.A.; Humber, M. MODIS Collection 5.1 Burned Area Product—MCD45, User's Guide Version 3.0.1. Available online: https://earthdata.nasa.gov/sites/default/files/field/document/MODIS_Burned_Area_Collection51_User_Guide_3.0.pdf (accessed on 26 October 2013).